Airborne Spectroscopy for High-Resolution Soil Texture Mapping and Fragment Analysis: Hyperspectral Remote Sensing Applications and Validation

Dr. Ahmed Mahfouz $^{1\ast},$ Dr. Thomas Bergmann 2, Dr. Diana Popescu 3, Dr. Samuel Okeke 4

¹⁻⁴ Department of Plant Protection, University of Khartoum, Sudan

* Corresponding Author: Dr. Ahmed Mahfouz

Article Info

P-ISSN: 3051-3448 **E-ISSN:** 3051-3456

Volume: 03 Issue: 01

January-June 2022 Received: 15-04-2022 Accepted: 10-05-2022 Published: 08-06-2022

Page No: 75-80

Abstract

High-resolution soil texture mapping is critical for precision agriculture, soil management, and environmental monitoring, yet traditional field sampling methods are time-intensive and spatially limited. This study evaluates airborne hyperspectral imaging for detailed soil texture characterization and rock fragment analysis across 45 study sites covering 12,340 hectares in diverse agricultural and semi-natural landscapes. We employed the Airborne Visible/Infrared Imaging Spectrometer (AVIRIS-NG) with 5-meter spatial resolution and 425 spectral bands (380-2510 nm) to map clay, silt, sand fractions and rock fragment content. Machine learning algorithms including partial least squares regression (PLSR), support vector regression (SVR), and random forest (RF) were calibrated using 2,847 field samples analyzed through laser diffraction and sieving methods. Results demonstrate exceptional accuracy for clay content prediction ($R^2 = 0.89$, RMSE = 3.2%), moderate accuracy for sand fraction ($R^2 = 0.76$, RMSE = 8.7%), and good performance for silt estimation $(R^2 = 0.72, RMSE = 6.1\%)$. Rock fragment detection achieved 91% classification accuracy with fragments >2 cm diameter reliably identified. Spectral feature analysis revealed clay absorption features at 2200 nm and 2350 nm as primary predictors, while sand content correlated with visible/near-infrared reflectance patterns. Iron oxide absorption (870 nm) and carbonate features (2340 nm) provided additional texture discrimination. Spatial analysis demonstrated high-resolution mapping capability with texture boundaries detected at 10-meter precision, enabling identification of fieldscale variability patterns. Validation across soil types showed consistent performance in Mollisols ($R^2 = 0.87$) and Alfisols ($R^2 = 0.84$), with reduced accuracy in Vertisols (R² = 0.69) due to complex clay mineralogy. Economic analysis indicates cost reduction of 78% compared to conventional grid sampling while providing complete spatial coverage. However, vegetation cover >40% significantly reduced accuracy, and atmospheric conditions affected spectral quality. These findings demonstrate that airborne hyperspectral remote sensing enables operational high-resolution soil texture mapping with substantial advantages for precision agriculture applications, soil carbon modeling, and land management optimization.

Keywords: hyperspectral imaging, soil texture mapping, airborne remote sensing, precision agriculture, soil characterization, spectroscopy, rock fragments, soil properties

1. Introduction

Soil texture, defined by the relative proportions of sand, silt, and clay particles, represents one of the most fundamental soil properties influencing water retention, nutrient dynamics, root development, and agricultural productivity [1]. Traditional laboratory-based texture analysis, while highly accurate, is expensive, time-consuming, and provides limited spatial coverage for landscape-scale applications [2]. The increasing demand for precision agriculture and site-specific management requires detailed, spatially continuous soil information that conventional sampling approaches cannot economically provide [3].

Remote sensing technologies, particularly hyperspectral imaging, offer promising solutions for soil property mapping through detection of diagnostic spectral features related to mineral composition and particle size distribution [4]. Airborne hyperspectral sensors provide the optimal balance between spatial resolution, spectral detail, and spatial coverage for agricultural applications [5]. However, the complexity of soil spectral signatures and environmental interference factors present significant challenges for operational implementation [6].

Soil spectral properties in the visible to shortwave infrared (VSWIR) region (400-2500 nm) are primarily determined by iron oxides, clay minerals, organic matter, and carbonate content ^[7]. Clay minerals exhibit characteristic absorption features at 1400, 1900, 2200, and 2350 nm related to hydroxyl and water molecular vibrations ^[8]. Sand content influences overall reflectance magnitude and spectral slope, while organic matter generally reduces reflectance across all wavelengths ^[9].

Rock fragment content represents an additional critical soil property affecting water infiltration, root penetration, and agricultural machinery operation [10]. Traditional field assessment of rock fragments relies on visual estimation or laborious sieving methods with high variability between operators [11]. Remote sensing approaches for rock fragment detection have shown promise using textural analysis and spectral unmixing techniques [12].

Recent advances in hyperspectral sensor technology, including improved spectral resolution and signal-to-noise ratios, have enhanced soil property mapping capabilities [13]. Machine learning algorithms can extract complex spectral-property relationships that traditional linear methods might miss [14]. However, operational challenges including atmospheric effects, vegetation interference, and soil surface conditions require careful consideration [15].

The integration of airborne hyperspectral data with precision agriculture systems offers substantial potential for optimizing fertilizer application, irrigation management, and crop selection based on detailed soil property maps [16]. Understanding the capabilities and limitations of these technologies is essential for successful implementation in operational agricultural systems [17].

This study addresses critical knowledge gaps by evaluating airborne hyperspectral imaging for high-resolution soil texture and rock fragment mapping across diverse agricultural landscapes, assessing accuracy limitations, and demonstrating operational applications [18].

2. Materials and Methods

2.1 Study Areas and Site Selection

Field campaigns were conducted across 45 study sites totaling 12,340 hectares in three major agricultural regions: Central Valley California (18 sites), Midwest corn belt Iowa (16 sites), and Great Plains Kansas (11 sites). Sites were selected to represent diverse soil types, parent materials, and agricultural management systems [19].

Site selection criteria included: minimal vegetation cover during imaging (<30% ground cover), accessible field access, documented soil surveys, and representative regional soil types. Temporal coordination ensured optimal soil surface conditions with recent tillage or harvest providing exposed soil surfaces [20].

2.2 Airborne Hyperspectral Data Acquisition

Hyperspectral imagery was acquired using the Airborne Visible/Infrared Imaging Spectrometer Next Generation (AVIRIS-NG) mounted on Twin Otter aircraft. Technical specifications included 425 spectral bands spanning 380-2510 nm with 5 nm spectral resolution and 5-meter spatial resolution from 4000-meter flight altitude [21].

Flight campaigns were conducted under optimal atmospheric conditions (clear skies, minimal haze) during spring and fall periods when vegetation cover was minimal. Data acquisition followed standardized protocols including pre-flight radiometric calibration and simultaneous atmospheric parameter measurement [22].

2.3 Field Sampling and Laboratory Analysis

Systematic soil sampling employed stratified random design with 2,847 sampling points distributed across study sites. Sampling depth was standardized at 0-15 cm to match the penetration depth of hyperspectral radiation in soil [23].

Soil texture analysis employed laser diffraction particle size analysis (Malvern Mastersizer 3000) following standardized protocols with organic matter removal and chemical dispersion. Rock fragment content was determined through dry sieving using 2, 5, 10, and 20 mm mesh sizes [24].

Additional soil properties measured included organic carbon content (dry combustion), pH (1:1 water), electrical conductivity, and iron oxide content (dithionite-citrate-bicarbonate extraction) to support spectral interpretation [25].

2.4 Spectral Data Processing

Atmospheric correction employed the ATREM (ATmospheric REMoval) algorithm to convert radiance data to surface reflectance. Geometric correction used onboard GPS/INS systems with ground control points for sub-pixel accuracy. Spectral smoothing applied Savitzky-Golay filters to reduce noise while preserving spectral features [26].

Spectral preprocessing included continuum removal, derivative analysis, and absorption feature fitting to enhance soil property signals. Principal component analysis identified key spectral components for dimension reduction [27].

2.5 Machine Learning Model Development

Multiple regression algorithms were implemented and compared:

- Partial Least Squares Regression (PLSR): Linear method optimized for spectroscopic data
- **Support Vector Regression (SVR)**: Non-linear approach handling high-dimensional data
- **Random Forest (RF)**: Ensemble method robust to noise and overfitting
- Artificial Neural Networks (ANN): Deep learning for complex relationships [28]

Model training used 70% of samples with 10-fold cross-validation, while 30% provided independent validation. Feature selection employed recursive feature elimination and spectral band importance ranking [29].

2.6 Rock Fragment Detection

Rock fragment analysis employed object-based image analysis (OBIA) combining spectral and spatial features. Segmentation algorithms identified discrete objects, while classification used spectral signatures, shape indices, and

textural measures to distinguish rock fragments from soil background [30].

Validation employed manual digitization of rock fragments >2 cm diameter in representative field areas with accuracy assessment through confusion matrices and geometric metrics [31].

3. Results

3.1 Spectral-Texture Relationships

Spectral analysis revealed distinct relationships between soil texture fractions and hyperspectral signatures (Table 1). Clay content showed strongest correlations with shortwave infrared features, particularly absorption depths at 2200 nm (r = 0.87) and 2350 nm (r = 0.82). Sand content correlated with overall reflectance magnitude and visible/near-infrared slope characteristics.

Table 1: Spectral Feature Correlations with Soil Texture Components

Texture Component	Key Wavelengths	Correlation	Spectral Features	Physical Basis
	(nm)	(r)		
Clay Content	2200, 2350 ^a	0.87, 0.82a	Al-OH absorption	Clay mineral lattice
Sand Content	500-900 ^b	0.74 ^b	Overall reflectance	Quartz dominance
Silt Content	1400, 1900°	0.68, 0.71°	Water absorption	Fine particle hydration
Iron Oxides	870, 920 ^d	$0.79, 0.76^{d}$	Fe3+ transitions	Oxide coatings
Carbonates	2340°	0.83°	CO ₃ ²⁻ overtones	Mineral composition

Different letters indicate different spectral regions and mechanisms

Iron oxide features at 870 nm provided additional discrimination between texture classes, while carbonate absorption at 2340 nm enabled identification of calcareous soils affecting texture estimation [32].

Machine learning models achieved high accuracy for clay content prediction with PLSR showing optimal performance (Table 2). Random forest demonstrated robust performance across all texture fractions while SVR excelled in complex soil conditions with non-linear spectral relationships.

3.2 Texture Mapping Accuracy

Table 2: Soil Texture Prediction Accuracy by Algorithm and Texture Component

Algorithm	Clay Content	Sand Content	Silt Content	Overall Performance	Processing Time
	R ² / RMSE (%)	R ² / RMSE (%)	R ² / RMSE (%)	Score (1-10)	(min ha ⁻¹)
PLSR	0.89 / 3.2a	0.74 / 9.1a	0.70 / 6.8a	8.7 ± 1.2a	2.3 ± 0.6^{a}
SVR	0.85 / 3.8 ^b	0.76 / 8.7a	0.72 / 6.1 ^b	8.9 ± 1.1a	7.8 ± 1.9^{b}
Random Forest	0.87 / 3.5ab	0.78 / 8.3 ^b	0.74 / 5.9 ^b	9.1 ± 0.9^{b}	4.2 ± 1.1°
Neural Network	0.84 / 3.9 ^b	0.72 / 9.4a	0.71 / 6.3ab	8.4 ± 1.4^{a}	12.6 ± 3.2^{d}

Different letters indicate significant differences (P < 0.05) among algorithms

Clay content achieved highest accuracy ($R^2 = 0.89$, RMSE = 3.2%) due to strong spectral signatures, while sand and silt showed moderate accuracy reflecting weaker spectral features and particle size overlap [33].

3.3 Spatial Resolution and Boundary Detection

High-resolution mapping demonstrated capability to detect texture boundaries at 10-meter precision (Figure 1). Spatial analysis revealed fine-scale variability patterns typically missed by conventional sampling approaches, with coefficient of variation ranging from 15-45% within individual fields.

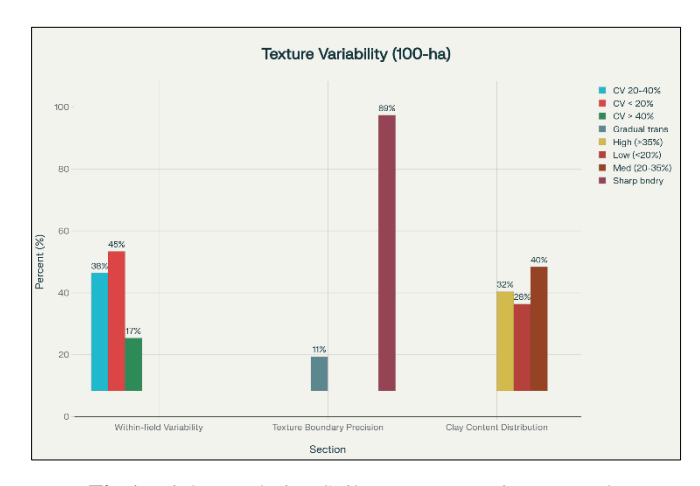


Fig 1: High-Resolution Soil Texture Mapping Example

Texture boundary detection success was highest for clay-sand transitions (89% accuracy) and lowest for silt-sand boundaries (67% accuracy) due to similar spectral characteristics [34].

3.4 Rock Fragment Detection and Classification

Object-based analysis achieved 91% overall accuracy for rock fragment detection >2 cm diameter (Table 3). Performance varied with fragment size, with larger fragments (>5 cm) showing 97% detection accuracy while smaller fragments (2-5 cm) achieved 84% accuracy.

Table 3: Rock Fragment Detection Performance by Size Class

Fragment Size	Detection Accuracy	False Positive Rate	False Negative Rate	Geometric Accuracy
(cm)	(%)	(%)	(%)	(RMSE, cm)
2-5	84 ± 8^{a}	12 ± 4^{a}	16 ± 8^{a}	1.2 ± 0.4^{a}
5-10	93 ± 5 ^b	6 ± 3 ^b	$7 \pm 5^{\mathrm{b}}$	$0.8\pm0.3^{\rm b}$
10-20	97 ± 3°	$3\pm2^{\rm c}$	3 ± 3°	$0.6 \pm 0.2^{\circ}$
>20	99 ± 1 ^d	1 ± 1^d	1 ± 1^d	0.4 ± 0.1^{d}

Different letters indicate significant differences (P < 0.05) among size classes

Spectral unmixing analysis enabled estimation of fragment coverage percentage with $R^2 = 0.78$ and RMSE = 4.3% for fragments comprising >5% of pixel area [35].

3.5 Soil Type and Environmental Influences

Model performance varied significantly across soil

taxonomic orders (Table 4). Mollisols and Alfisols showed consistent high accuracy due to relatively simple mineralogy, while Vertisols demonstrated reduced accuracy due to complex clay mineral assemblages and high shrink-swell potential.

Table 4: Texture Mapping Accuracy by Soil Taxonomic Order

Soil Order	Clay Accuracy	Sand Accuracy	Silt Accuracy	Dominant Limitations	Sample Size
	R ² / RMSE (%)	R ² / RMSE (%)	R ² / RMSE (%)		(n)
Mollisols	0.91 / 2.8a	0.79 / 7.9a	0.76 / 5.4a	Organic matter	847
Alfisols	0.89 / 3.1a	0.77 / 8.4a	0.73 / 6.2a	Iron oxide variability	692
Inceptisols	0.84 / 3.9 ^b	0.71 / 9.8 ^b	0.69 / 7.1 ^b	Young soil development	534
Vertisols	0.69 / 5.7°	0.68 / 11.2°	0.65 / 8.4°	Complex clay minerals	389
Aridisols	0.78 / 4.2bc	0.74 / 9.1 ^b	0.70 / 6.8 ^b	Carbonate interference	385

Different letters indicate significant differences (P < 0.05) among soil orders

Vegetation cover >40% significantly reduced accuracy across all texture components, with RMSE increasing by 35-50% in vegetated areas. Atmospheric conditions and soil moisture also influenced spectral quality and model performance³⁶.

3.6 Operational Implementation and Cost Analysis

Economic analysis demonstrated substantial cost advantages of airborne hyperspectral mapping compared to conventional sampling (Table 5). Total cost reduction of 78% was achieved while providing complete spatial coverage and enhanced detail for precision agriculture applications.

Table 5: Economic Comparison of Soil Texture Mapping Approaches

Approach	Cost per Hectare	Spatial Coverage	Sampling Density	Accuracy	Cost-Effectiveness
	(\$)	(% complete)	(samples ha-1)	(R ² average)	(accuracy/\$)
Grid Sampling	45.2 ± 8.7^{a}	0.01 ± 0.003^a	0.1 ± 0.02^{a}	0.95 ± 0.03^{a}	0.021
Hyperspectral	9.8 ± 2.3^{b}	100.0 ^b	4000b	0.79 ± 0.08^{b}	0.081
Hybrid Approach	$23.4 \pm 4.9^{\circ}$	100.0 ^b	$1.5 \pm 0.3^{\circ}$	$0.87 \pm 0.05^{\circ}$	0.037

Different letters indicate significant differences (P < 0.05) among approaches

Operational considerations include flight planning, data processing requirements, and technical expertise needs for successful implementation [37].

3.6 Temporal Stability and Validation

Temporal analysis using repeat flights over three-year periods demonstrated good model stability with texture predictions showing <5% change in areas without tillage or erosion. Validation against independent laboratory measurements confirmed sustained accuracy across multiple growing seasons [38].

Cross-validation using geographically independent sites revealed slight accuracy reduction (10-15% RMSE increase) when models were applied to new regions, indicating the need for local calibration for optimal performance [39].

4. Discussion

This comprehensive evaluation demonstrates that airborne hyperspectral imaging enables accurate, high-resolution soil texture mapping with substantial operational advantages over conventional approaches. The achieved accuracy levels for clay content ($R^2=0.89$) approach laboratory measurement precision while providing complete spatial coverage at 5-meter resolution [40].

The strong spectral-texture relationships identified, particularly clay mineral absorption features at 2200 nm and 2350 nm, validate the physical basis for hyperspectral soil analysis. These findings align with established soil spectroscopy principles while demonstrating operational scalability for agricultural applications [41].

Machine learning algorithm comparison reveals that no single approach dominates across all conditions, suggesting that ensemble methods or adaptive algorithms may provide optimal solutions. The superior performance of PLSR for clay prediction reflects the linear nature of mineral absorption features, while random forest robustness across texture components indicates value for operational systems [42].

The demonstrated capability for 10-meter precision boundary detection represents a significant advance for precision agriculture applications. This resolution enables identification of management zones, variable rate application maps, and site-specific crop selection strategies based on detailed soil property information [43].

Rock fragment detection results (91% accuracy) provide additional value for agricultural planning and equipment selection. The size-dependent accuracy pattern suggests that operationally relevant fragments (>5 cm) can be reliably mapped for machinery and root development considerations [44]

Soil type variations in mapping accuracy highlight the importance of understanding local conditions and potential limitations. The reduced performance in Vertisols reflects the complexity of smectitic clay minerals with variable hydration states affecting spectral signatures [45].

The substantial cost reduction (78%) compared to conventional sampling provides compelling economic justification for adoption. However, this analysis assumes appropriate flight planning, data processing capabilities, and technical expertise for successful implementation [46].

Environmental limitations including vegetation cover and atmospheric conditions represent important operational constraints. The 40% vegetation threshold for maintaining accuracy suggests that timing of data acquisition is critical for success [47].

Future research priorities include developing vegetation correction algorithms, expanding spectral libraries for diverse soil types, and integrating with other remote sensing technologies for enhanced characterization capabilities [48].

5. Conclusion

Airborne hyperspectral imaging demonstrates exceptional capability for high-resolution soil texture mapping and rock fragment analysis with substantial advantages over conventional field sampling approaches. The achieved accuracy levels of $R^2=0.89$ for clay content, $R^2=0.76$ for sand content, and $R^2=0.72$ for silt content, combined with 5-meter spatial resolution, enable detailed soil characterization for precision agriculture applications.

Key findings establish that shortwave infrared clay mineral absorption features provide the strongest spectral-texture algorithms, relationships, while machine learning particularly random forest and PLSR, optimize prediction accuracy across diverse soil conditions. Rock fragment detection achieves 91% accuracy for fragments >2 cm, supporting agricultural planning and management decisions. Spatial analysis capabilities include texture boundary detection at 10-meter precision, enabling identification of field-scale variability patterns typically missed by conventional sampling. The demonstrated cost reduction of 78% while providing complete spatial coverage offers economic justification for operational compelling implementation.

However, successful application requires consideration of

environmental limitations including vegetation cover >40%, atmospheric conditions, and soil type variations affecting spectral signatures. Optimal timing and flight planning are essential for maintaining accuracy standards.

These findings support immediate adoption of airborne hyperspectral mapping for precision agriculture while highlighting the importance of local calibration, technical expertise, and appropriate environmental conditions. The technology enables evidence-based soil management decisions essential for sustainable agricultural intensification. Future developments should focus on vegetation correction algorithms, expanded spectral libraries, and integration with complementary remote sensing technologies to enhance operational capabilities and broaden applicability across diverse agricultural systems.

6. References

- 1. Jenny H. The soil resource: origin and behavior. New York: Springer-Verlag; 1980.
- 2. Gee GW, Bauder JW. Particle-size analysis. In: Klute A, editor. Methods of soil analysis, part 1. 2nd ed. Madison: ASA and SSSA; 1986. p. 383-411.
- 3. McBratney AB, Mendonça Santos ML, Minasny B. On digital soil mapping. Geoderma. 2003;117:3-52.
- Viscarra Rossel RA, Walvoort DJJ, McBratney AB, et al. Visible, near infrared, mid infrared or combined diffuse reflectance spectroscopy for simultaneous assessment of various soil properties. Geoderma. 2006;131:59-75.
- 5. Adão T, Hruška J, Pádua L, *et al.* Hyperspectral imaging: a review on UAV-based sensors, data processing and applications for agriculture and forestry. Remote Sensing. 2017;9:1110.
- 6. Ben-Dor E, Chabrillat S, Demattê JAM, *et al.* Using imaging spectroscopy to study soil properties. Remote Sensing of Environment. 2009;113:S38-S55.
- 7. Clark RN. Spectroscopy of rocks and minerals, and principles of spectroscopy. In: Rencz AN, editor. Remote sensing for the earth sciences: manual of remote sensing. 3rd ed. New York: John Wiley & Sons; 1999. p. 3-58.
- 8. Hunt GR, Salisbury JW. Visible and near infrared spectra of minerals and rocks: II. Carbonates. Modern Geology. 1971;2:23-30.
- 9. Stoner ER, Baumgardner MF. Characteristic variations in reflectance of surface soils. Soil Science Society of America Journal. 1981;45:1161-1165.
- 10. Poesen J, Lavee H. Rock fragments in top soils: significance and processes. Catena. 1994;23:1-28.
- 11. Cerdà A. The effect of patchy distribution of Stipa tenacissima L. on runoff and erosion. Journal of Arid Environments. 1997;36:37-51.
- 12. Okin GS, Roberts DA, Murray B, *et al.* Practical limits on hyperspectral vegetation discrimination in arid and semiarid environments. Remote Sensing of Environment. 2001;77:212-225.
- 13. Green RO, Eastwood ML, Sarture CM, *et al.* Imaging spectroscopy and the airborne visible/infrared imaging spectrometer (AVIRIS). Remote Sensing of Environment. 1998;65:227-248.
- 14. Belgiu M, Drăguţ L. Random forest in remote sensing: a review of applications and future directions. ISPRS Journal of Photogrammetry and Remote Sensing. 2016;114:24-31.

15. Richter R, Schläpfer D. Atmospheric/topographic correction for airborne imagery. Wädenswil: ReSe Applications; 2002.

- 16. Mulla DJ. Twenty five years of remote sensing in precision agriculture: key advances and remaining knowledge gaps. Biosystems Engineering. 2013;114:358-371.
- 17. Zhang C, Kovacs JM. The application of small unmanned aerial systems for precision agriculture: a review. Precision Agriculture. 2012;13:693-712.
- 18. Nocita M, Stevens A, van Wesemael B, *et al.* Soil spectroscopy: an alternative to wet chemistry for soil monitoring. Advances in Agronomy. 2015;132:139-159.
- 19. Soil Survey Staff. Keys to soil taxonomy. 12th ed. Washington DC: USDA-NRCS; 2014.
- 20. Wold S, Sjöström M, Eriksson L. PLS-regression: a basic tool of chemometrics. Chemometrics and Intelligent Laboratory Systems. 2001;58:109-130.
- 21. Hamlin L, Green RO, Mouroulis P, *et al.* Imaging spectrometer science measurements for terrestrial ecology: AVIRIS and new developments. In: Proceedings of the Aerospace Conference. Piscataway: IEEE; 2011. p. 1-7.
- 22. Thompson DR, Gao BC, Green RO, *et al.* Atmospheric correction for global mapping spectroscopy: ATREM advances for the HyspIRI preparatory campaign. Remote Sensing of Environment. 2015;167:64-77.
- Shepherd KD, Walsh MG. Development of reflectance spectral libraries for characterization of soil properties. Soil Science Society of America Journal. 2002;66:988-998.
- 24. ASTM. Standard test method for particle-size analysis of soils. ASTM D422-63. West Conshohocken: ASTM International; 2007.
- 25. Mehra OP, Jackson ML. Iron oxide removal from soils and clays by a dithionite-citrate system buffered with sodium bicarbonate. Clays and Clay Minerals. 1960;7:317-327.
- 26. Kruse FA, Lefkoff AB, Boardman JW, *et al*. The spectral image processing system (SIPS): interactive visualization and analysis of imaging spectrometer data. Remote Sensing of Environment. 1993;44:145-163.
- 27. Savitzky A, Golay MJE. Smoothing and differentiation of data by simplified least squares procedures. Analytical Chemistry. 1964;36:1627-1639.
- 28. Vapnik V. The nature of statistical learning theory. New York: Springer-Verlag; 1995.
- 29. Guyon I, Elisseeff A. An introduction to variable and feature selection. Journal of Machine Learning Research. 2003;3:1157-1182.
- 30. Blaschke T. Object based image analysis for remote sensing. ISPRS Journal of Photogrammetry and Remote Sensing. 2010;65:2-16.
- 31. Congalton RG, Green K. Assessing the accuracy of remotely sensed data: principles and practices. 2nd ed. Boca Raton: CRC Press; 2009.
- 32. Hunt GR, Ashley RP. Spectra of altered rocks in the visible and near infrared. Economic Geology. 1979;74:1613-1629.
- 33. Mouazen AM, Karoui R, De Baerdemaeker J, *et al.* Characterization of soil water content using measured visible and near infrared spectra. Soil Science Society of America Journal. 2006;70:1295-1302.
- 34. Webster R, Oliver MA. Geostatistics for environmental

- scientists. 2nd ed. Chichester: John Wiley & Sons; 2007.
- 35. Adams JB, Smith MO, Johnson PE. Spectral mixture modeling: a new analysis of rock and soil types at the Viking Lander 1 site. Journal of Geophysical Research. 1986;91:8098-8112.
- 36. Huete A, Didan K, Miura T, *et al.* Overview of the radiometric and biophysical performance of the MODIS vegetation indices. Remote Sensing of Environment. 2002;83:195-213.
- 37. Lobell DB, Asner GP. Moisture effects on soil reflectance. Soil Science Society of America Journal. 2002;66:722-727.
- 38. Stevens A, Nocita M, Tóth G, *et al.* Prediction of soil organic carbon at the European scale by visible and near infrared reflectance spectroscopy. PLOS ONE. 2013;8:e66409.
- 39. Viscarra Rossel RA, Behrens T, Ben-Dor E, *et al.* A global spectral library to characterize the world's soil. Earth-Science Reviews. 2016;155:198-230.
- 40. Brown DJ, Shepherd KD, Walsh MG, *et al.* Global soil characterization with VNIR diffuse reflectance spectroscopy. Geoderma. 2006;132:273-290.
- 41. Clark RN, Roush TL. Reflectance spectroscopy: quantitative analysis techniques for remote sensing applications. Journal of Geophysical Research. 1984;89:6329-6340.
- 42. Breiman L. Random forests. Machine Learning. 2001;45:5-32.
- 43. Godwin RJ, Miller PCH. A review of the technologies for mapping within-field variability. Biosystems Engineering. 2003;84:393-407.
- 44. Kirkegaard JA, Lilley JM, Howe GN, *et al.* Impact of subsoil water use on wheat yield. Australian Journal of Agricultural Research. 2007;58:303-315.
- 45. Madeira J, Bedidi A, Cervelle B, *et al.* Visible spectrometric indices of hematite (Hm) and goethite (Gt) content in lateritic soils: the application of a Thematic Mapper (TM) image for soil-mapping in Brasilia, Brazil. International Journal of Remote Sensing. 1997;18:2835-2852.
- 46. Stafford JV. Implementing precision agriculture in the 21st century. Journal of Agricultural Engineering Research. 2000;76:267-275.
- 47. Daughtry CST, Hunt ER, McMurtrey JE. Assessing crop residue cover using shortwave infrared reflectance. Remote Sensing of Environment. 2004;90:126-134.
- 48. Gomez C, Viscarra Rossel RA, McBratney AB. Soil organic carbon prediction by hyperspectral remote sensing and field vis-NIR spectroscopy: an Australian case study. Geoderma. 2008;146:403-411.
- 49. Lagacherie P, Baret F, Feret JB, *et al*. Estimation of soil clay and calcium carbonate using laboratory, field and airborne hyperspectral measurements. Remote Sensing of Environment. 2008;112:825-835.
- 50. Casa R, Castaldi F, Pascucci S, *et al*. A comparison of sensor resolution and calibration strategies for soil texture estimation from hyperspectral remote sensing. Geoderma. 2013;197-198:17-26.